THE JOURNAL OF PHYSICAL CHEMISTRY A
A JOURNAL OF THE AMERICAN CHEMICAL SOCIETY

pubs.acs.org/JPCA Article

Effect of a Single Platinum Atom within a Small Metal Oxide Cluster: Reaction of DMMP with Size-Selected $Pt_1Zr_2O_7$ Supported on HOPG

Michael A. Denchy, Linjie Wang, Benjamin R. Bilik, Lucas Hansen, Sandra Albornoz, Francisco Lizano, and Kit H. Bowen*

Cite This: J. Phys. Chem. A 2023, 127, 2895−2901 Read Online

ACCESS | Metrics & More | Article Recommendations

ABSTRACT: Chemical warfare agents (CWAs) are a persistent threat facing civilians and military personnel across the modern geopolitical landscape. The development of the next generation of protective and sensing materials stands to benefit from an improved fundamental understanding of the interaction of CWA molecules with the active components of such candidate materials. The use of model systems in well-controlled environments offers a route to glean such information and has been applied here to investigate the fundamental interaction of a nerve agent simulant molecule, dimethyl methylphosphonate (DMMP), with a small cluster model of a single atom catalyst (SAC) active site. The cluster models, $Pt_1Zr_2O_7$, were prepared by depositing mass-selected cluster anions synthesized in the gas phase onto a 100 K highly oriented pyrolytic graphite (HOPG) substrate surface prepared in ultra-high vacuum (UHV) at sub-monolayer coverage. Upon deposition, the cluster anions lost their charge to the electrically conductive surface to yield free-standing neutral clusters. The HOPG-supported clusters were characterized by X-ray photoelectron spectroscopy (XPS) to determine the oxidation states and chemical environment of the metal atoms present within the clusters. The reactivity of the clusters with DMMP was investigated via temperature-programmed desorption/reaction (TPD/R) and XPS experiments in which the clusters were exposed to DMMP and incrementally heated to higher temperatures. In contrast to two other HOPG-supported clusters, $(ZrO_2)_3$ and $Pt_1Ti_2O_7$, recently investigated in our laboratory, $Pt_1Zr_2O_7$ decomposed DMMP to primarily evolve a methane species, which was completely absent for the other clusters.

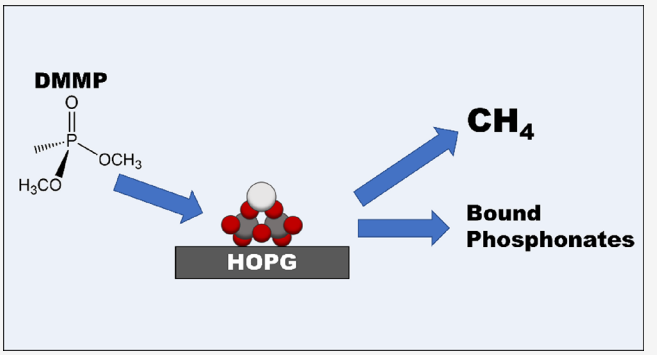

INTRODUCTION

Chemical warfare agents (CWAs) are a persistent threat to military personnel and civilians across the modern geopolitical landscape. There is a pressing need for a deeper understanding of the fundamental interaction between these lethal molecules and the active components of materials employed for their destruction, mitigation, and detection.[1] An especially dangerous class of CWAs is the family of organophosphorus nerve agents, which are among the most lethal chemicals ever synthesized by humans.[2] Due to their extremely high toxicity and the need for tight governmental regulation to prevent their proliferation, civilian research laboratories are relegated to the use of simulant molecules, which mimic some key aspects of live agents, but are much less dangerous to handle. A commonly employed simulant for investigating the surface adsorption and decomposition properties of agents like sarin is dimethyl methylphosphonate (DMMP). DMMP has been employed to investigate the potential adsorption and decomposition properties of a wide array of metal and metal oxide model systems, including Pt(111),[3] Ni(111), and Pd(111),[4] and Al_2O_3,[5,6] and TiO_2,[7−11] among numerous others.

In recent years, particular attention has been paid to a class of metal organic frameworks (MOFs) that offer a potential route to the realization of an active material distinct from the metal oxide particle-impregnated activated carbon materials in the current generation of CWA protective equipment.[12,13] Such MOFs are composed of an organic scaffolding of linker ligands constructed between metal or metal oxide nodes, which can serve as active sites for CWA binding and decomposition chemistry. In particular, a highly active node consisting of a partially hydroxylated zirconium oxide hexamer cluster has been shown to facilitate the hydrolysis of various nerve agent

Received: December 27, 2022
Revised: March 8, 2023
Published: March 23, 2023

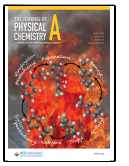

https://doi.org/10.1021/acs.jpca.2c08783
J. Phys. Chem. A 2023, 127, 2895−2901

simulants when incorporated into a host of MOF structures.[14−23] Moreover, bulk zirconium hydroxide has also shown promise in the adsorption and decomposition of various nerve agent simulants and live agents as well.[24−27] This work motivated a recent study of ours in which we investigated the reactivity of even smaller ZrO_2 trimer clusters size-selected in the gas phase and soft-landed onto an HOPG substrate surface in ultra-high vacuum (UHV). It was found that DMMP was strongly adsorbed by the clusters and proceeded to decompose with heating, evolving primarily methanol along with relatively minor amounts of dimethyl ether and formaldehyde.[28]

While the use of small metal oxide particles and clusters as active decomposition species has been a research focus for some time now, a recently emerging newer focus is on the potential application of single catalytically active metal atoms supported on the surface of metal oxide particles to this problem. Over the last decade, the concept of such a single atom catalyst (SAC) was convincingly demonstrated in a seminal study by Qiao et al.[29] and spawned a field that has grown exponentially in scope since.[30] Their application to the problem of CWA decomposition is thus an exciting new area and one that promises to reveal important new physical insights. A recently developed experimental approach within our laboratory involves the modeling of SAC active sites by small clusters, size-selected in the gas phase and soft-landed onto a support surface, in which a small metal oxide moiety is doped with a single metal atom. A schematic illustrating this concept is shown below in Scheme 1.

Scheme 1. Illustration Showing a Bulk Metal-Oxide Supported Single Atom Catalyst and a Corresponding Small Cluster Model

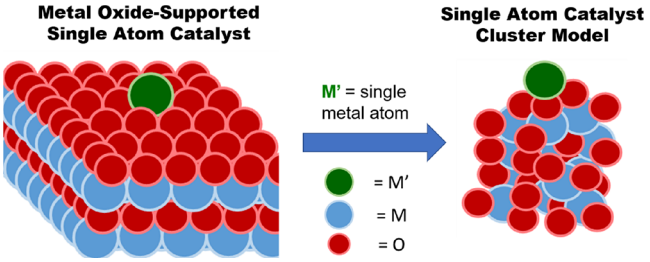

The intention is for the metal oxide moiety to serve as a small portion of the bulk metal oxide support of a conventional SAC material. However, the realization of properties diverging from their bulk counterparts for such small SAC cluster models would constitute an important insight in and of itself, as such clusters can be potentially incorporated into materials like MOFs as active nodes. Hence, the properties of the SAC cluster models and their interaction with various molecules is a worthy line of research, which offers to supplement the vastly growing body of SAC-related work.

Here, we apply our approach to investigate the interaction of DMMP with an SAC cluster model of single atom Pt on Zr oxide, i.e., $Pt_1Zr_2O_7$. $Pt_1Zr_2O_7^-$ cluster anions were synthesized in the gas phase via a magnetron sputtering/inert gas condensation source and soft-landed with low kinetic energy (<1 eV/atom) onto a prepared HOPG substrate in UHV, following mass selection by an in-line quadrupole mass filter (QMF). The supported clusters were characterized via X-ray photoelectron spectroscopy (XPS) to confirm their identity and elucidate the oxidation states of their constituent atoms. The reactivity of the clusters with DMMP was then explored via temperature-programmed desorption/reaction (TPD/R) and in situ XPS measurements following DMMP exposure and incremental heating to several elevated temperatures. A schematic summarizing this experimental approach is shown below in Scheme 2.

Scheme 2. Conceptual Overview of Size-Selected Cluster Deposition and Reactivity of Experiments

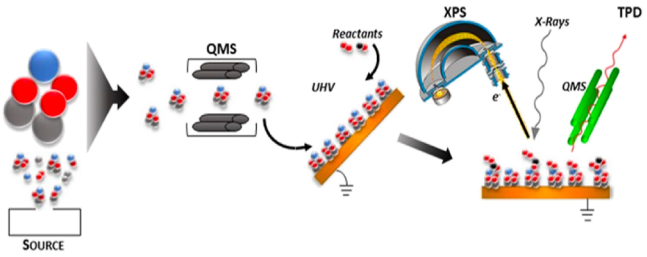

These experiments revealed a decomposition chemistry distinct from the HOPG-supported $(ZrO_2)_3$ clusters studied previously, as well as recent experiments of ours involving another comparable SAC cluster model, $Pt_1Ti_2O_7$.[31] Unlike those clusters, the HOPG-supported $Pt_1Zr_2O_7$ clusters were found to primarily evolve methane, directly resulting from DMMP decomposition. Similar to the reactivity observed for $Pt_1Ti_2O_7$, evolution of CO and H_2 resulting from DMMP decomposition was observed as well.

EXPERIMENTAL METHODS

Supported Cluster Sample Preparation. A highly detailed description of the apparatus used to prepare size-selected supported cluster samples and investigate their reactivity was reported previously.[32] An overview of the method used to synthesize, mass-select, and deposit the clusters onto a prepared substrate in UHV will thus be described here in brief. Cluster ions were synthesized in the gas phase via a combined magnetron sputtering/inert gas condensation source. For magnetron sputtering, a metal sputtering target is fixed above a cylindrical permanent magnet and biased to a negative voltage (−200−400 V) and Ar gas is flowed into the source, generating Ar^+ cations, which sputter the target surface. The sputtered neutral and charged atoms and particles are entrained in a flow of He, which serves as a buffer gas for inducing clustering within the inert gas condensation volume and carrying the clusters out of the source. Ar (Airgas, 99.999%) and He (Airgas, 99.999%) are introduced into the source as a mixture via precision dosing valves (Leybold 28341), each with a backing pressure of 30 psi. The mixture was seeded with a small amount of pure O_2 (Airgas, 99.994%) via a micro-flow valve (INFICON, VDH016-x) having a backing pressure of 15 psi to enable reactive sputtering, enhancing the formation of metal oxide cluster ions. The cluster ions formed are then transported by a series of multipole ion guides and electrostatic optics, with the anions separated from the cations via a 90° quadrupole deflector. The separated anions are then transmitted through a QMF (Extrel, 440 kHz, 19 mm diam. rods) for mass analysis and mass selection, followed by guided deposition onto the substrate surface under soft-landing conditions (<1 eV/atom). Upon deposition, the cluster ions lost their charge to the

https://doi.org/10.1021/acs.jpca.2c08783
J. Phys. Chem. A 2023, 127, 2895−2901

electrically conductive, grounded substrate, resulting in a discharge current that was measured via a picoammeter (Keithley 6514). This current was measured over time and integrated to determine the total number of clusters deposited onto the surface over the course of a deposition, assuming one unit of elementary charge (1e = 1.602×10^{-19} Coulombs) per cluster.

The cluster anions for these experiments, $Pt_1Zr_2O_7^-$, were synthesized via reactive magnetron sputtering of a pure Zr metal target (Kurt J. Lesker, Grade 702) with several thin Pt strips (1 × 10 mm) spot-welded into the sputter-etched "racetrack" of the target. The cluster anions were deposited onto an HOPG substrate (Brucker, ZYB Grade, 12 × 12 mm^2, 2 mm thickness) prepared via mechanical exfoliation in air and rapidly transferred into UHV. The HOPG substrate was further cleaned by annealing in vacuo (T = 773 K, Δt = 50 min) prior to all experiments. The substrate was mounted onto a sample holder consisting of an inverted UHV thermocouple/power feedthrough (Kurt J. Lesker, TFT1KY2C302) attached to a hollow sample holder column mounted on a UHV 4-axis manipulator system (McAllister Technical Services). Ta foil pouches were wrapped around the feedthrough power leads and used to secure the substrate, while a chromel and alumel thermocouple wire junction was attached to the thermocouple leads and spring-loaded against the back of the substrate. Samples were cooled via thermal contact with a liquid nitrogen reservoir within the sample holder column.

Samples of DMMP (Sigma-Aldrich, ≥98%) were prepared by loading a vessel with 1−2 mL of liquid and attaching it to a bakeable stainless steel vapor dosing setup. The DMMP samples were purified via several freeze−pump−thaw cycles using liquid nitrogen to remove any dissolved atmospheric gases. The presence of any additional H_2O was further minimized via constant pumping on the sample vessel for ∼1 h while simultaneously cooling the vessel with an ice-water bath just prior to dosing.

XPS. The XPS setup used in these experiments was composed of a non-monochromatic Mg/Al dual-node X-ray source (Perkin-Elmer PHI 04-548) and a hemispherical energy analyzer (Perkin-Elmer PHI 10-360), taken from a refurbished commercial XPS system (Perkin-Elmer PHI 5100), and mounted onto the surface analytical chamber of our apparatus with a manufacture specified offset angle of 54.7°. XPS measurements were acquired using Mg Kα X-rays (1256.3 eV) to induce core electron photoemission in the samples, which were positioned with the surface plane of the HOPG substrate oriented normal to the inlet aperture of the hemispherical analyzer, i.e., at a 90° take-off angle. All XPS spectra reported in this study were calibrated to a graphitic carbon 1s (C 1s) binding energy value of 284.5 eV. Quantitative data analysis and peak model fitting of all spectra were performed using CasaXPS (Casa Software Ltd.) software.

C 1s spectra were fitted using two peak components following Shirley background subtraction, namely, an asymmetric Gaussian-broadened Lorentzian peak (A(0.4,0.38,20)-GL(20)) for the C 1s transition arising from sp^2-hybridized graphitic carbon and a symmetric Gaussian-broadened Lorentzian peak (GL(30)) for the higher binding energy feature near ∼291 eV arising from the well-known $\pi-\pi^*$ transition in a well-ordered HOPG surface. A full width at half maximum (FWHM) of ∼1.6 eV was obtained for the sp^2 C 1s peaks in all spectra. Phosphorus 2p (P2p) spectra were fitted using sets of Gaussian-broadened Lorentzian (GL(30)) spin-orbit doublets following linear background subtraction and constrained to have a spin-orbit splitting of 0.87 eV and an integrated peak area ratio of 2:1, corresponding to the $2p_{3/2}$ and $2p_{1/2}$ states. Platinum 4f (Pt 4f) and zirconium 3d (Zr 3d) spectra were each fitted with sets of Gaussian-broadened Lorentzian (GL(30)) spin-orbit doublets following Shirley background subtraction. Each Pt 4f doublet was constrained to have a spin-orbit splitting of 3.33 eV and an integrated peak area ratio of 4:3, corresponding to the $4f_{7/2}$ and $4f_{5/2}$ states. Each Zr 3d doublet was constrained to have a spin-orbit splitting of 2.43 eV and an integrated peak area ratio of 3:2, corresponding to the $3d_{5/2}$ and $3d_{3/2}$ states. The constraints for each species were maintained for the fitting of all XPS spectra, which were acquired using a constant analyzer pass energy of 71.55 eV.

Temperature-Programmed Desorption/Reaction. TPD/R experiments were performed by heating the prepared samples at a well-controlled linear rate of 1 K/s, while simultaneously monitoring the species desorbing from the surface via a line-of-sight commercial residual gas analyzer/quadrupole mass spectrometer (QMS; Hiden HAL/3F PIC). The QMS consists of a low-profile electron bombardment ionization source, mass-selecting quadrupole with pre- and post-filters, and a single-channel secondary electron multiplier pulse-counting detector. During the experiments, the samples were placed within several millimeters of the inlet to the ionization source of the QMS, and operation using multiplex mode allowed effectively simultaneous monitoring of up to 15 different mass-to-charge ratio (m/z) values. Linear temperature-programming of the samples was accomplished via resistive heating of the HOPG substrate using the current generated by an external power supply (Sorensen DCS 55-55) driven by a programmable PID controller (Eurotherm 2048) interfaced with a thermocouple temperature−voltage converter (Dataexel, DAT4531A) connected to the K-type thermocouple spring-loaded against the back of the HOPG substrate for monitoring the substrate temperature.

The QMS was also used to ensure the purity of DMMP doses for all experiments, with simultaneous monitoring of a major fragment (m/z = 79) and the parent ion (m/z = 124) of DMMP, as well as other fragments and potential contaminant species. During a typical dose, DMMP was introduced into the chamber via a UHV-compatible variable leak valve (Varian, 951-5106) until reaching a measured QMS signal of ∼2×10^4 counts for m/z = 79 and maintained at that level for 100 s. After exposure to DMMP, all samples were heated linearly to 298 K and maintained at that temperature for 2 min to remove the majority of DMMP physisorbed on the HOPG substrate surface. After this initial treatment, the samples were rapidly cooled back down to 100 K and positioned within close proximity of the QMS for a TPD/R run.

RESULTS AND DISCUSSION

Characterization of HOPG-Supported $Pt_1Zr_2O_7$ Clusters. HOPG-supported cluster samples for each experiment were prepared by depositing 4×10^{13} mass-selected $Pt_1Zr_2O_7^-$ cluster anions onto HOPG at 100 K. A mass spectrum acquired for the cluster anion beam for typical source conditions used during sample preparation is shown in Figure 1.

From past experience, the cluster anion beam formed via reactive magnetron sputtering of pure Zr with O_2 does not exhibit any species within at least ±10 amu of the feature

https://doi.org/10.1021/acs.jpca.2c08783
J. Phys. Chem. A 2023, 127, 2895−2901

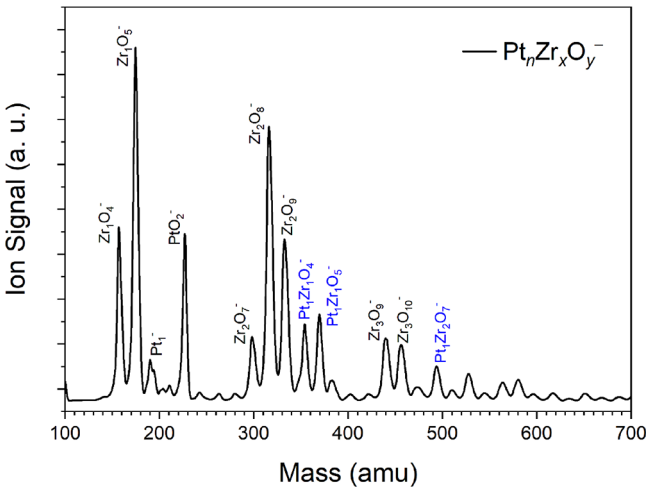

Figure 1. Mass spectrum acquired for a beam of $Pt_1Zr_2O_7^-$ cluster anions formed via reactive magnetron sputtering of a Pt/Zr sputtering target with O_2.

assigned to $Pt_1Zr_2O_7$ in Figure 1. Thus, we can be confident that by mass-selecting this species, we are exclusively selecting a single Pt atom-containing cluster anion for deposition.

XPS measurements collected for a typical $Pt_1Zr_2O_7$/HOPG sample after heating to 298 K for two minutes immediately following preparation are shown in Figure 2.

The spectrum acquired for the Pt 4f region is adequately fitted by two sets of *f*-orbital spin-orbit doublets corresponding to the $4f_{7/2}$ and $4f_{5/2}$ states of Pt. The fitted features are consistent with Pt^{2+} and Pt^{4+}, with a $4f_{7/2}$ binding energy of 72.6 and 74.5 eV, respectively.[33] The Pt atoms on the clusters are primarily present in the Pt^{2+} state. The spectrum acquired for the Zr 3d region is adequately fitted by one set of *d*-orbital spin-orbit doublets corresponding to the $3d_{5/2}$ and $3d_{3/2}$ states of Zr. The fitted feature is consistent with fully oxidized Zr^{4+}, with a $3d_{5/2}$ binding energy of 182.0 eV.[34,35] These XPS measurements are consistent with the thoroughly oxygenated clusters expected based on the assigned stoichiometry from the mass spectrum and support the Pt atom in the clusters being bound to oxygen atoms, rather than directly to Zr atoms.[36]

Reactivity of $Pt_1Zr_2O_7$/HOPG with DMMP. In order to investigate the reactivity of DMMP with the HOPG-supported $Pt_1Zr_2O_7$ clusters, a TPD/R experiment was performed. DMMP was exposed to prepared cluster samples at 100 K and then pre-treated to 298 K to remove excess DMMP physisorbed to the HOPG substrate, followed by a linear temperature ramp to 773 K. The primary result of this experiment was the evolution of methane, indicated by a desorption feature for m/z = 16. The signal measured for m/z = 16 during this experiment is shown in Figure 3 and is compared with that measured for DMMP exposed to bare HOPG and another single Pt atom-containing metal oxide cluster recently studied by our group, $Pt_1Ti_2O_7$.

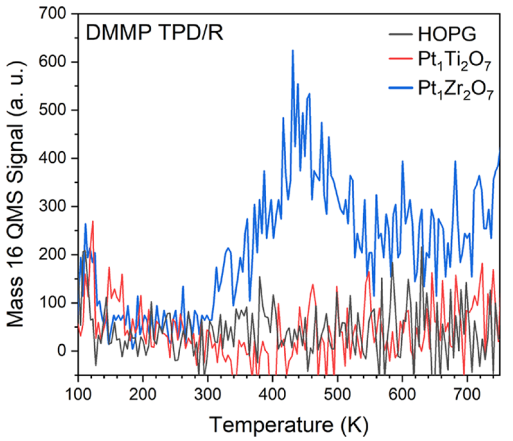

Figure 3. Comparison of TPD/R spectra acquired m/z = 16 for DMMP-exposed samples of $Pt_1Zr_2O_7$/HOPG (blue), $Pt_1Ti_2O_7$/HOPG (red), and HOPG without clusters (gray).

Notably, no methane evolution is observed for DMMP exposed to bare HOPG without $Pt_1Zr_2O_7$ clusters present, and neither is it observed for $Pt_1Ti_2O_7$ clusters, which were found to decompose DMMP into H_2O, CO, and H_2.[31] Another previous study of ours investigating the adsorption and decomposition of DMMP by HOPG-supported $(ZrO_2)_3$ clusters, which can be viewed as a species in which the single Pt atom is switched with a Zr atom, likewise saw no methane evolution. In that case, DMMP was primarily decomposed into methanol, with relatively minor amounts of dimethyl ether and formaldehyde evolved as well. Clearly, the presence of the single Pt atom on such small clusters can cause a dramatic change in the observed reactivity with a molecule like DMMP,

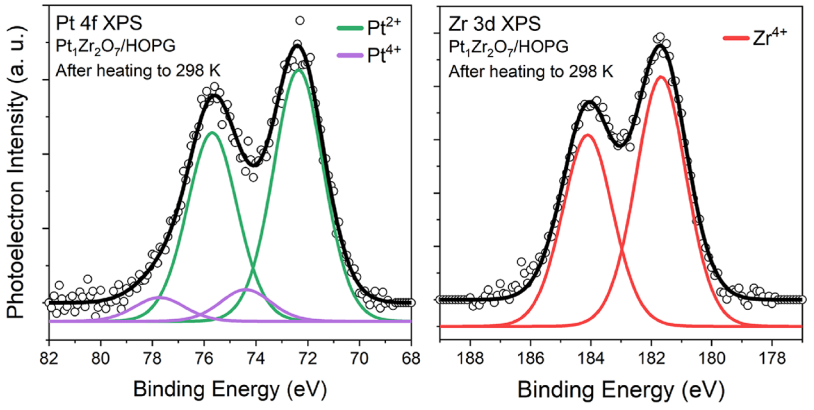

Figure 2. XPS spectra acquired for the Pt 4f (left) and Zr 3d (right) regions for $Pt_1Zr_2O_7$/HOPG prepared at 100 K and subsequently heated to 298 K. The Pt 4f spectrum is fitted with two spin-orbit doublets corresponding to Pt^{2+} (green) and Pt^{4+} (purple) states. The Zr 3d spectrum is fitted with one spin-orbit doublet corresponding to a fully oxidized Zr^{4+} state.

https://doi.org/10.1021/acs.jpca.2c08783
J. Phys. Chem. A 2023, 127, 2895−2901

but changes in the identity of the oxide metal, even to a different metal of the same family, can have substantial effects as well.

To further investigate the interaction between DMMP and the $Pt_1Zr_2O_7$ clusters, a series of XPS measurements were carried out after exposing the $Pt_1Zr_2O_7$/HOPG sample to DMMP at 100 K, followed by incremental heating to various temperatures. The spectrum acquired for the P 2p region after exposure of the $Pt_1Zr_2O_7$ clusters to DMMP at 100 K and heating to 298 K is shown in Figure 4.

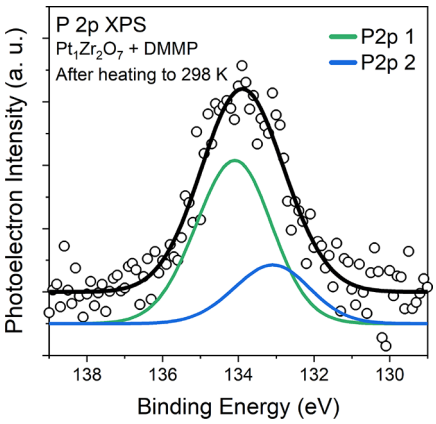

Figure 4. P 2p XPS spectrum acquired for DMMP-exposed $Pt_1Zr_2O_7$/HOPG at 100 K and after heating to 298 K. The spectrum has been fitted with two sets of spin-orbit doublets indicating distinguishable P 2p states, assigned to chemisorbed DMMP (green) and P-containing decomposition species (blue).

An adequate fit for the data was achieved using two sets of *p*-orbital spin-orbit doublets. For clarity, the envelope of each doublet is shown in the spectrum in Figure 4 and are labeled P2p1 and P2p2. P2p1 exhibits a $2p_{3/2}$ binding energy of 133.9 eV, which is typical of molecularly chemisorbed DMMP. This has been observed in previous studies of ours, as well as the work of others.[37,38] P2p2 exhibits a lower $2p_{3/2}$ binding energy of 132.9 eV, which has been previously assigned to surface-bound phosphonate or phosphate decomposition products.[8,39] This result shows that DMMP has already begun to decompose by room temperature and is similar to the results of our previous experiments involving room-temperature exposure of $(ZrO_2)_3$ clusters to DMMP.[28]

The results of the P2p XPS measurements after heating to each temperature are summarized in Figure 5.

Here, the relative amounts of P2p1 and P2p2 in relation to the total P2p signal measured, determined via the integrated peak area for each feature in the spectrum acquired for each heating temperature, are shown. From 298 to 473 K, there is an inversion of the major surface-bound species present, with decomposed DMMP dominating over chemisorbed DMMP. Further heating to as high as 673 K does not result in a significant change to the relative amount of each species present. The slight change observed can be due to the desorption of some P-containing decomposition species from the clusters at elevated temperatures, which cannot be ruled out entirely. Hence, while DMMP decomposition has occurred after heating to room temperature, much more extensive decomposition occurs upon heating to a higher temperature of 473 K. Notably, the peak desorption temperature measured for the major decomposition product observed for DMMP

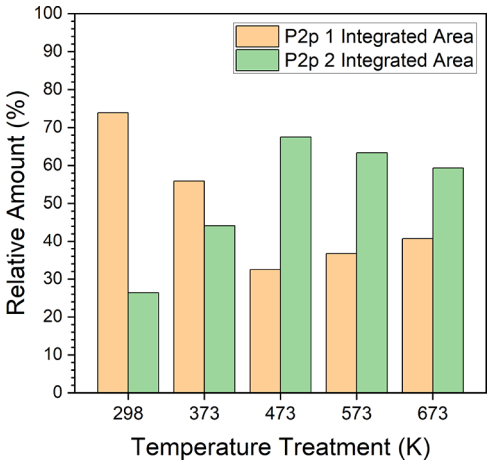

Figure 5. Comparison of the integrated peak areas for P2p1 (orange) and P2p2 (green) relative to the total P2p signal measured, after heating the DMMP-exposed $Pt_1Zr_2O_7$/HOPG sample to each indicated temperature.

decomposition during the TPD/R experiment was 450 K. Taken together, these results strongly suggest that the observed evolution of methane during TPD/R is directly correlated with the observed decomposition of DMMP via XPS.

The results of the XPS measurements acquired for the Pt 4f and Zr 3d regions after exposure of the $Pt_1Zr_2O_7$ cluster to DMMP at 100 K and heating to each temperature are shown in Figure 6.

The measurements acquired at each temperature are compared to those acquired in a separate control experiment for a sample of $Pt_1Zr_2O_7$ clusters prepared in the same fashion, but without any exposure to DMMP. In principle, this allows for the elucidation of any measurable effect on the Pt and Zr atoms in the clusters due to the adsorbed DMMP and any bound decomposition species present. Initially, the Pt $4f_{7/2}$ and the Zr $3d_{5/2}$ features are shifted to a higher binding energy slightly by 0.1 eV. Then, with heating, the Pt 4f feature experiences a monotonic shift lower in binding energy to 71.7 eV, while the Zr 3d feature experiences a monotonic shift higher in binding energy. In both cases, the DMMP-exposed samples mimic the same trend, with the Zr 3d feature experiencing a greater total shift higher in binding energy than the Pt 4f feature, relative to the bare cluster sample. This suggests that bound phosphonate decomposition species remaining after DMMP decomposition are bound to both Zr and Pt atoms in the clusters. Notably, there is no evidence for any reduction of Zr in the clusters, contrary to what we observed for Ti in our study of DMMP decomposition by HOPG-supported $Pt_1Ti_2O_7$ clusters. These two studies suggest that the role of the reducibility of the oxide metal can play a dramatic role in influencing the observed chemical reactivity of a system involving the same catalytic single metal atom. Moreover, the steering effects of reducibility are even manifest in the small-size limit of our SAC cluster models.

CONCLUSIONS

The soft landing of size-selected clusters was successfully employed to prepare samples of small cluster models of an SAC material composed of single Pt atoms on Zr oxide. The samples prepared by depositing $Pt_1Zr_2O_7^-$ onto the surface of a prepared HOPG substrate in UHV were characterized by

https://doi.org/10.1021/acs.jpca.2c08783
J. Phys. Chem. A 2023, 127, 2895−2901

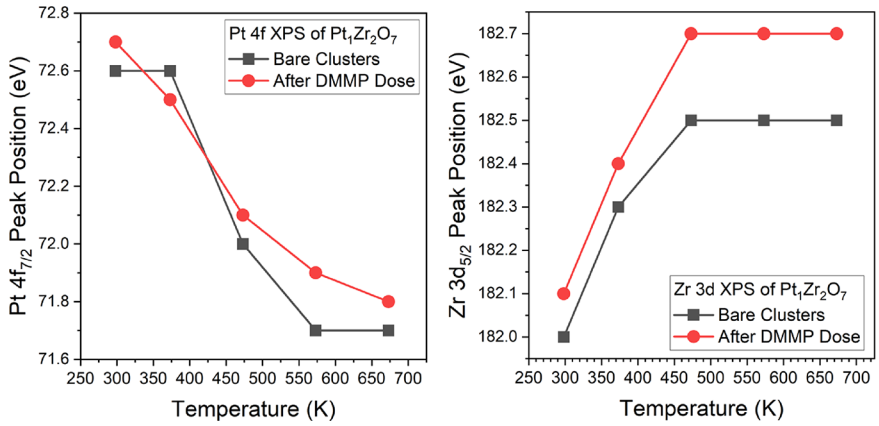

Figure 6. Comparison plot of the binding energies of apparent peak center for the spectral envelope acquired from XPS measurements of the Pt 4f (left) and Zr 3d (right) regions for the DMMP-exposed $Pt_1Zr_2O_7$/HOPG sample (red) and bare $Pt_1Zr_2O_7$/HOPG sample without DMMMP exposure (gray), after heating to the indicated temperatures.

XPS, showing single Pt atoms predominantly in the Pt^{2+} state bound to fully oxidized Zr^{4+} through shared oxygen atoms. This resembles the common binding motifs seen for well-characterized bulk metal oxide-supported SAC materials in which single Pt atoms are often anchored to oxygen atoms of the oxide surface. The reactivity of the $Pt_1Zr_2O_7$ clusters toward DMMP, a nerve agent simulant, was investigated by TPD/R and in situ XPS experiments and was found to be distinct from comparable metal oxide clusters studied within our laboratory containing only Zr atoms, $(ZrO_2)_3$, and a single Pt atom bound to a Ti oxide moiety, $Pt_1Ti_2O_7$. Methane was found to be the primary volatile reaction product observed for DMMP-exposed $Pt_1Zr_2O_7$ clusters, while no detectable methane evolution was observed for the other clusters. Moreover, XPS measurements showed strong adsorption of P-containing decomposition species after heating to as high as 773 K for the $Pt_1Zr_2O_7$ clusters, similar to that observed for $(ZrO_2)_3$ clusters, but in stark contrast to the $Pt_1Ti_2O_7$ clusters where the desorption of P-containing decomposition species was observed in XPS and TPD/R experiments. Clearly, the presence of a single Pt atom, as well as the choice of partner in the accompanying metal oxide moiety, for reactive species at the smallest size limit, can have a dramatic effect on the exhibited reactivity.

AUTHOR INFORMATION

Corresponding Author

Kit H. Bowen − *Department of Chemistry, Johns Hopkins University, Baltimore, Maryland 21218, United States;* orcid.org/0000-0002-2858-6352; Email: kbowen@jhu.edu

Authors

Michael A. Denchy − *Department of Chemistry, Johns Hopkins University, Baltimore, Maryland 21218, United States;* orcid.org/0000-0002-2757-8705

Linjie Wang − *Department of Chemistry, Johns Hopkins University, Baltimore, Maryland 21218, United States;* orcid.org/0000-0002-6558-1753

Benjamin R. Bilik − *Department of Chemistry, Johns Hopkins University, Baltimore, Maryland 21218, United States*

Lucas Hansen − *Department of Chemistry, Johns Hopkins University, Baltimore, Maryland 21218, United States*

Sandra Albornoz − *Department of Chemistry, Johns Hopkins University, Baltimore, Maryland 21218, United States*

Francisco Lizano − *Department of Chemistry, Johns Hopkins University, Baltimore, Maryland 21218, United States*

Complete contact information is available at: https://pubs.acs.org/10.1021/acs.jpca.2c08783

Notes

The authors declare no competing financial interest.

ACKNOWLEDGMENTS

This material is based upon work supported by the Army Research Office (ARO) under Grant Number W911NF2020207.

REFERENCES

(1) Kim, K.; Tsay, O. G.; Atwood, D. A.; Churchill, D. G. Destruction and Detection of Chemical Warfare Agents. *Chem. Rev.* **2011**, *111*, 5345−5403.

(2) Munro, N. Toxicity of the Organophosphate Chemical Warfare Agents GA, GB, and VX: Implications for Public Protection. *Environ. Health Persp.* **1994**, *102*, 18−37.

(3) Henderson, M. A.; White, J. M. Adsorption and Decomposition of Dimethyl Methylphosphonate on Platinum(111). *J. Am. Chem. Soc.* **1988**, *110*, 6939−6947.

(4) Guo, X.; Yoshinobu, J.; Yates, J. T. Decomposition of an Organophosphonate Compound (Dimethylmethylphosphonate) on the Nickel(111) and Palladium(111) Surfaces. *J. Phys. Chem.* **1990**, *94*, 6839−6842.

(5) Templeton, M. K.; Weinberg, W. H. Adsorption and Decomposition of Dimethyl Methylphosphonate on an Aluminum Oxide Surface. *J. Am. Chem. Soc.* **1985**, *107*, 97−108.

(6) Aurian-Blajeni, B.; Boucher, M. M. Interaction of Dimethyl Methylphosphonate with Metal Oxides. *Langmuir* **1989**, *5*, 170−174.

(7) Rusu, C. N.; Yates, J. T. Adsorption and Decomposition of Dimethyl Methylphosphonate on TiO_2. *J. Phys. Chem. B* **2000**, *104*, 12292−12298.

(8) Zhou, J.; Varazo, K.; Reddic, J. E.; Myrick, M. L.; Chen, D. A. Decomposition of Dimethyl Methylphosphonate on TiO_2(110): Principal Component Analysis Applied to X-Ray Photoelectron Spectroscopy. *Anal. Chim. Acta* **2003**, *496*, 289−300.

(9) Trubitsyn, D. A.; Vorontsov, A. V. Experimental Study of Dimethyl Methylphosphonate Decomposition over Anatase TiO_2. *J. Phys. Chem. B* **2005**, *109*, 21884−21892.

(10) Kim, C. S.; Lad, R. J.; Tripp, C. P. Interaction of Organophosphorous Compounds with TiO_2 and WO_3 Surfaces

Probed by Vibrational Spectroscopy. *Sens. Actuators, B* **2001**, *76*, 442−448.
(11) Panayotov, D. A.; Morris, J. R. Uptake of a Chemical Warfare Agent Simulant (DMMP) on TiO_2: Reactive Adsorption and Active Site Poisoning. *Langmuir* **2009**, *25*, 3652−3658.
(12) Park, S. H.; McClain, S.; Tian, Z. R.; Suib, S. L.; Karwacki, C. Surface and Bulk Measurements of Metals Deposited on Activated Carbon. *Chem. Mater.* **1997**, *9*, 176−183.
(13) Morrison, R. W. *NBC Filter Performance*; U.S. Army Soldier and Biological Chemical Command: Aberdeen Proving Ground, MD, 2001.
(14) Ryu, S. G.; Kim, M.-K.; Park, M.; Jang, S. O.; Kim, S. H.; Jung, H. Availability of Zr-Based MOFs for the Degradation of Nerve Agents in All Humidity Conditions. *Microporous Mesoporous Mater.* **2019**, *274*, 9−16.
(15) Moon, S.-Y.; Proussaloglou, E.; Peterson, G. W.; DeCoste, J. B.; Hall, M. G.; Howarth, A. J.; Hupp, J. T.; Farha, O. K. Detoxification of Chemical Warfare Agents Using a Zr_6-Based Metal−Organic Framework/Polymer Mixture. *Chem. − Eur. J.* **2016**, *22*, 14864−14868.
(16) Mondloch, J. E.; Katz, M. J.; Isley, W. C., III; Ghosh, P.; Liao, P.; Bury, W.; Wagner, G. W.; Hall, M. G.; DeCoste, J. B.; Peterson, G. W.; et al. Destruction of Chemical Warfare Agents Using Metal−Organic Frameworks. *Nature Mater* **2015**, *14*, 512−516.
(17) Liu, Y.; Moon, S.-Y.; Hupp, J. T.; Farha, O. K. Dual-Function Metal−Organic Framework as a Versatile Catalyst for Detoxifying Chemical Warfare Agent Simulants. *ACS Nano* **2015**, *9*, 12358−12364.
(18) Moon, S.-Y.; Wagner, G. W.; Mondloch, J. E.; Peterson, G. W.; DeCoste, J. B.; Hupp, J. T.; Farha, O. K. Effective, Facile, and Selective Hydrolysis of the Chemical Warfare Agent VX Using Zr_6-Based Metal−Organic Frameworks. *Inorg. Chem.* **2015**, *54*, 10829−10833.
(19) Katz, M. J.; Moon, S.-Y.; Mondloch, J. E.; Beyzavi, M. H.; Stephenson, C. J.; Hupp, J. T.; Farha, O. K. Exploiting Parameter Space in MOFs: A 20-Fold Enhancement of Phosphate-Ester Hydrolysis with UiO-66-NH2. *Chem. Sci.* **2015**, *6*, 2286−2291.
(20) Moon, S.-Y.; Liu, Y.; Hupp, J. T.; Farha, O. K. Instantaneous Hydrolysis of Nerve-Agent Simulants with a Six-Connected Zirconium-Based Metal−Organic Framework. *Angewandte Chemie International Edition* **2015**, *54*, 6795−6799.
(21) Wang, G.; Sharp, C.; Plonka, A. M.; Wang, Q.; Frenkel, A. I.; Guo, W.; Hill, C.; Smith, C.; Kollar, J.; Troya, D.; et al. Mechanism and Kinetics for Reaction of the Chemical Warfare Agent Simulant, DMMP(g), with Zirconium(IV) MOFs: An Ultrahigh-Vacuum and DFT Study. *J. Phys. Chem. C* **2017**, *121*, 11261−11272.
(22) Peterson, G. W.; Moon, S.-Y.; Wagner, G. W.; Hall, M. G.; DeCoste, J. B.; Hupp, J. T.; Farha, O. K. Tailoring the Pore Size and Functionality of UiO-Type Metal−Organic Frameworks for Optimal Nerve Agent Destruction. *Inorg. Chem.* **2015**, *54*, 9684−9686.
(23) Troya, D. Reaction Mechanism of Nerve-Agent Decomposition with Zr-Based Metal Organic Frameworks. *J. Phys. Chem. C* **2016**, *120*, 29312−29323.
(24) Jeon, S.; Schweigert, I. V.; Pehrsson, P. E.; Balow, R. B. Kinetics of Dimethyl Methylphosphonate Adsorption and Decomposition on Zirconium Hydroxide Using Variable Temperature In Situ Attenuated Total Reflection Infrared Spectroscopy. *ACS Appl. Mater. Interfaces* **2020**, *12*, 14662−14671.
(25) Balow, R. B.; Lundin, J. G.; Daniels, G. C.; Gordon, W. O.; McEntee, M.; Peterson, G. W.; Wynne, J. H.; Pehrsson, P. E. Environmental Effects on Zirconium Hydroxide Nanoparticles and Chemical Warfare Agent Decomposition: Implications of Atmospheric Water and Carbon Dioxide. *ACS Appl. Mater. Interfaces* **2017**, *9*, 39747−39757.
(26) Bandosz, T. J.; Laskoski, M.; Mahle, J.; Mogilevsky, G.; Peterson, G. W.; Rossin, J. A.; Wagner, G. W. Reactions of VX, GD, and HD with Zr(OH)4: Near Instantaneous Decontamination of VX. *J. Phys. Chem. C* **2012**, *116*, 11606−11614.
(27) Jeon, S.; Balow, R. B.; Daniels, G. C.; Ko, J. S.; Pehrsson, P. E. Conformal Nanoscale Zirconium Hydroxide Films for Decomposing Chemical Warfare Agents. *ACS Appl. Nano Mater.* **2019**, *2*, 2295−2307.
(28) Denchy, M. A.; Wang, L.; Blando, N.; Hansen, L.; Bilik, B. R.; Tang, X.; Hicks, Z.; Gantefoer, G.; Bowen, K. H. Adsorption and Decomposition of Dimethyl Methylphosphonate on Size-Selected Zirconium Oxide Trimer Clusters. *J. Phys. Chem. C* **2021**, *125*, 23688−23698.
(29) Qiao, B.; Wang, A.; Yang, X.; Allard, L. F.; Jiang, Z.; Cui, Y.; Liu, J.; Li, J.; Zhang, T. Single-Atom Catalysis of CO Oxidation Using Pt_1/FeO_x. *Nature Chem* **2011**, *3*, 634−641.
(30) Kaiser, S. K.; Chen, Z.; Faust Akl, D.; Mitchell, S.; Pérez-Ramírez, J. Single-Atom Catalysts across the Periodic Table. *Chem. Rev.* **2020**, *120*, 11703−11809.
(31) Denchy, M. A.; Wang, L.; Hansen, L.; Bilik, B. R.; Albornoz, S.; Lizano, F.; Bowen, K. H. On the Nature of HOPG-Supported $Pt_1Ti_2O_7$ and Its Decomposition of a Nerve Agent Simulant: A Cluster Model of a Single Atom Catalyst Active Site. *Submitted to Phys. Chem. Chem. Phys.* **2022**.
(32) Denchy, M. A.; Wang, L.; Bilik, B. R.; Hansen, L.; Albornoz, S.; Lizano, F.; Blando, N.; Hicks, Z.; Ganteför, G. An Ultrasmall Cluster Model for Investigating Single Atom Catalysis: Dehydrogenation of 1-Propanamine by Size-Selected $Pt_1Zr_2O_7$ Clusters Supported on HOPG. *J. Phys. Chem. A* **2022**, *126*, 7578−7590.
(33) Li, J.; Guan, Q.; Wu, H.; Liu, W.; Lin, Y.; Sun, Z.; Ye, X.; Zheng, X.; Pan, H.; Zhu, J.; et al. Highly Active and Stable Metal Single-Atom Catalysts Achieved by Strong Electronic Metal−Support Interactions. *J. Am. Chem. Soc.* **2019**, *141*, 14515−14519.
(34) Kim, M.-S.; Ko, Y.-D.; Hong, J.-H.; Jeong, M.-C.; Myoung, J.-M.; Yun, I. Characteristics and Processing Effects of ZrO_2 Thin Films Grown by Metal-Organic Molecular Beam Epitaxy. *Appl. Surf. Sci.* **2004**, *227*, 387−398.
(35) Zhang, N. L.; Song, Z. T.; Wan, Q.; Shen, Q. W.; Lin, C. L. Interfacial and Microstructural Properties of Zirconium Oxide Thin Films Prepared Directly on Silicon. *Appl. Surf. Sci.* **2002**, *202*, 126−130.
(36) Li, H.; Choi, J.-I. J.; Mayr-Schmölzer, W.; Weilach, C.; Rameshan, C.; Mittendorfer, F.; Redinger, J.; Schmid, M.; Rupprechter, G. Growth of an Ultrathin Zirconia Film on Pt_3Zr Examined by High-Resolution X-Ray Photoelectron Spectroscopy, Temperature-Programmed Desorption, Scanning Tunneling Microscopy, and Density Functional Theory. *J. Phys. Chem. C* **2015**, *119*, 2462−2470.
(37) Head, A. R.; Tang, X.; Hicks, Z.; Wang, L.; Bleuel, H.; Holdren, S.; Trotochaud, L.; Yu, Y.; Kyhl, L.; Karslıoğlu, O.; Fears, K.; Owrutsky, J.; Zachariah, M.; Bowen, K. H.; Bluhm, H. Thermal Desorption of Dimethyl Methylphosphonate from MoO_3. *Catal., Struct. React.* **2017**, *3*, 112−118.
(38) Trotochaud, L.; Tsyshevsky, R.; Holdren, S.; Fears, K.; Head, A. R.; Yu, Y.; Karslıoğlu, O.; Pletincx, S.; Eichhorn, B.; Owrutsky, J.; et al. Spectroscopic and Computational Investigation of Room-Temperature Decomposition of a Chemical Warfare Agent Simulant on Polycrystalline Cupric Oxide. *Chem. Mater.* **2017**, *29*, 7483−7496.
(39) Wang, L.; Denchy, M.; Blando, N.; Hansen, L.; Bilik, B.; Tang, X.; Hicks, Z.; Bowen, K. H. Thermal Decomposition of Dimethyl Methylphosphonate on Size-Selected Clusters: A Comparative Study between Copper Metal and Cupric Oxide Clusters. *J. Phys. Chem. C* **2021**, *125*, 11348−11358.

https://doi.org/10.1021/acs.jpca.2c08783
J. Phys. Chem. A 2023, 127, 2895−2901